JACS
JOURNAL OF THE AMERICAN CHEMICAL SOCIETY
pubs.acs.org/JACS
Article

Red-Light-Induced Ligand-to-Metal Charge Transfer Catalysis by Tuning the Axial Coordination of Cobyrinate

Sajjad Dadashi-Silab, Cristina Preston-Herrera, Daniel G. Oblinsky, Gregory D. Scholes, and Erin E. Stache*

Cite This: J. Am. Chem. Soc. 2024, 146, 34583−34590
Read Online
ACCESS | Metrics & More | Article Recommendations | Supporting Information

ABSTRACT: Photoinduced ligand-to-metal charge transfer (LMCT) is a powerful technique for the formation of reactive radical species via homolytic cleavage of the metal−ligand bond. Here, we present that the excited state LMCT of a cobyrinate complex can be accessed by tuning its axial coordination with thiolates as ligands. We demonstrate the photoreduction of cobalt via the excited state Co−S bond homolytic cleavage, as guided by the DFT calculations, which signify the relevance of thiolate axial ligands facilitating the LMCT reactivity. By exploiting this excited state LMCT of cobyrinate, we developed a catalyst-controlled activator regeneration mechanism to catalyze an efficient atom transfer radical polymerization (ATRP) under low-energy light irradiation. Tuning the coordination sphere of cobyrinate provides further control over the electronic properties of the complex while also accessing photothermal conversion in mediating ATRP catalysis.

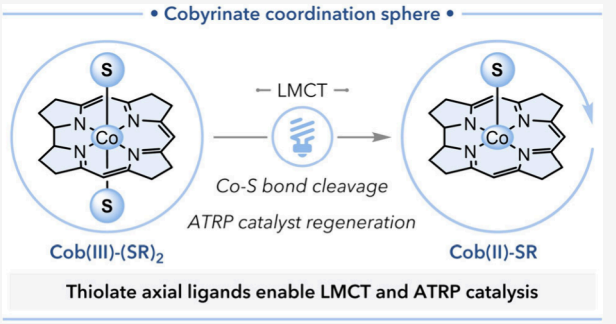

INTRODUCTION

Harnessing the power of light provides new, exciting opportunities for synthesizing complex (macro)molecules.[1−5] In photochemical processes, the absorption of photonic energy by a transition metal complex generates high-energy excited-state species to facilitate chemical transformations. Photocatalysts with long excited-state lifetimes engage in bimolecular outer-sphere interactions, forming reactive radical intermediates via single electron transfer, charge transfer, or hydrogen atom abstraction mechanisms. However, bimolecular interactions require long excited-state lifetimes, posing a limitation on exploring the photocatalytic reactivity of a wide range of transition metal complexes.[6,7] Therefore, identifying new mechanisms of harnessing visible light might enable elusive transformations.

We recently reported the utility of a new mode of harnessing visible light through photothermal conversion in multiple bond-forming and bond-breaking processes.[8−10] In photothermal conversion, the excitation event is followed by nonradiative relaxation pathways that generate heat.[11,12] The thermal gradients formed enable the selective activation of thermodynamically demanding transformations under mild conditions. We identified that cobyrinate, a hydrophobic derivative of vitamin B_{12}, acts as an efficient molecular photothermal conversion agent owing to its flexible structural properties and short excited state lifetimes.[13] The potential of cobyrinate as a dual photothermal conversion catalyst was realized by mediating cobalt-catalyzed atom transfer radical polymerization (ATRP).[14]

Despite achieving efficient photothermal reactivity across a wide range of wavelengths from visible to near-infrared light, the polymerization activity of cobyrinate decreased at low catalyst concentrations. This diminished reactivity is due to the deactivation of the catalyst by radical terminations that impeded the progress of polymerization, resulting in low monomer conversions (Figure 1). Therefore, an exogenous catalyst regeneration mechanism was identified to reactivate the catalyst and polymerization. Exogenous or initiating radicals could be generated using a UV/blue active photoinitiator. However, this strategy limits the full potential of cobyrinate as a polymerization catalyst under low-energy light irradiation (λ > 450 nm) due to the exogenous initiating system being independent of the catalyst.

We envisioned a catalyst-controlled mechanism that would facilitate activator regeneration using the catalyst's photochemical properties. Photoinduced ligand-to-metal charge transfer (LMCT) has emerged as a promising strategy for developing new reactivity of transition metal catalysts via

Received: September 7, 2024
Revised: November 12, 2024
Accepted: November 18, 2024
Published: December 10, 2024

https://doi.org/10.1021/jacs.4c12432
J. Am. Chem. Soc. 2024, 146, 34583−34590

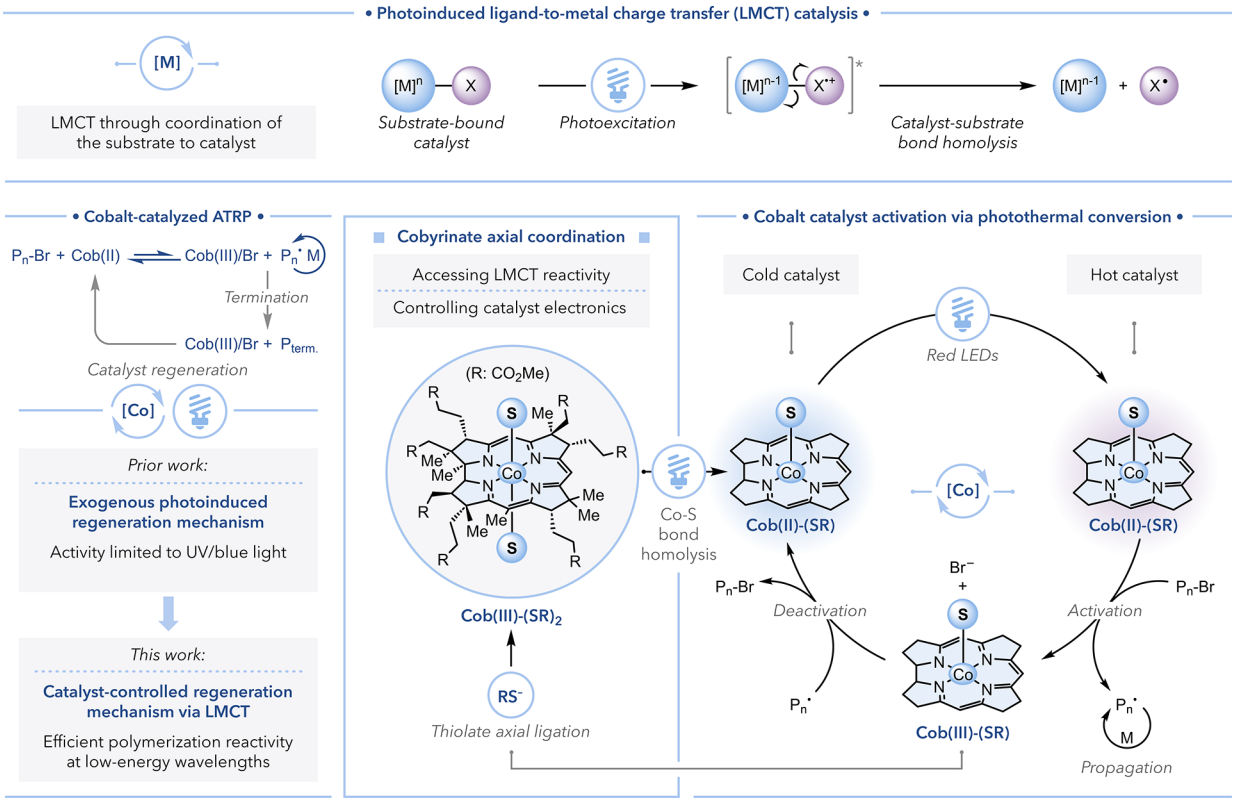

Figure 1. Photoinduced ligand-to-metal charge-transfer (LMCT) catalysis generates radical intermediates through the homolytic cleavage of the catalyst-substrate bond. Cobalt-catalyzed ATRP and the development of activator regeneration mechanisms: (prior work) an exogenous photoinitiating system with activity limited to UV/blue lights and (this work) a catalyst-controlled mechanism that enables in situ reduction of the catalyst via LMCT and achieves efficient polymerization across a wide range of wavelengths. Altering the axial coordination of cobyrinate using thiolates to access LMCT and control the electronic properties of the complex. Photothermal conversion enhances the activity of cobyrinate in mediating ATRP.

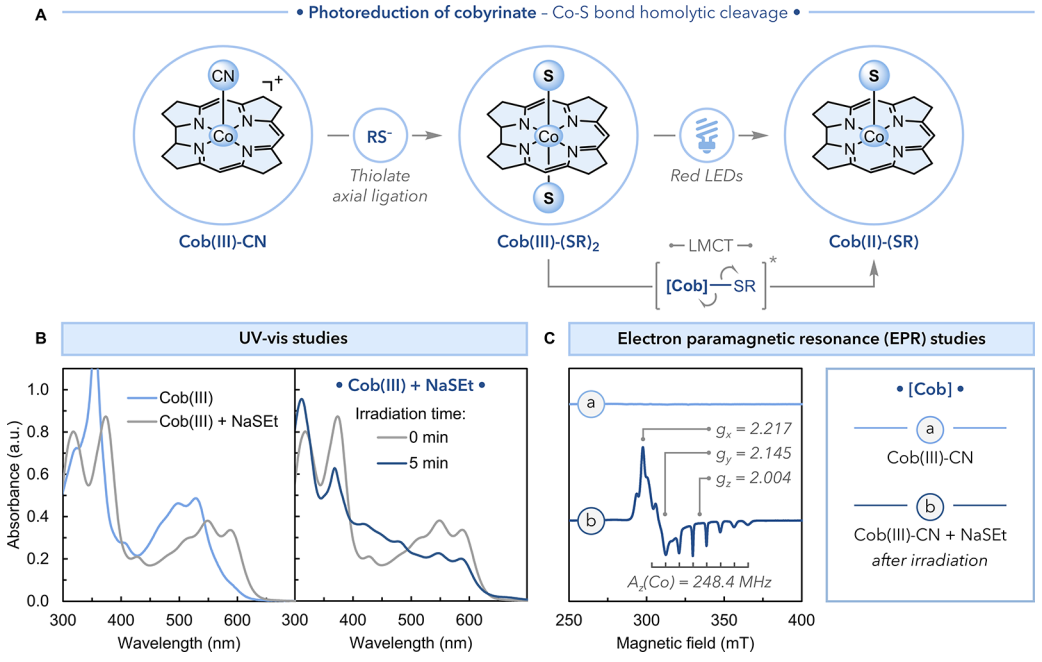

Figure 2. (A) Photoreduction of the cobyrinate complex through an LMCT process cleaving the Co−S bond. (B) UV−vis studies indicate coordination of the thiolate to Cob(III) (left panel), which can be subsequently reduced by red-light irradiation (630 nm, right panel). For UV−vis measurements: [Cob] = 50 μM, [NaSEt] = 500 μM in DMF. (C) Formation of a paramagnetic Cob(II) complex via photoreduction of the Cob(III)−thiolate complex as observed by the X-band EPR spectroscopy (simulation provided in SI).

https://doi.org/10.1021/jacs.4c12432
J. Am. Chem. Soc. 2024, 146, 34583−34590

unimolecular, inner-sphere excited state reactions (Figure 1).[15−18] This process involves the coordination of electron-rich, strongly donating substrates to high-valent metals, whose acceptor orbitals are populated in the excited state by a transfer of electron density from ligand-based orbitals. As a result, the substrate-bound catalyst undergoes homolytic cleavage and generates reactive radical intermediates while reducing the metal center.[19−33]

We propose that modifying the axial coordination of cobyrinate to promote excited state LMCT would result in photoreduction of the metal center. Here we investigate the reactivity of the Co−S bond formed by the coordination of thiolate ligands to cobyrinate through the axial positions.[34−37] Our strategy exploits the excited state reactivity of the Co−S bond, which undergoes a homolytic cleavage to generate the activator catalyst for ATRP across a wide range of wavelengths. We demonstrate that the coordination sphere of cobyrinate further allows tuning of the electronic properties of the catalyst. This effect, combined with the photothermal conversion properties of cobyrinate, offers a unique strategy for mediating highly efficient ATRP catalysis with low-energy irradiation (Figure 1).

RESULTS AND DISCUSSION

Photoreduction Studies. The monoanionic nature of the corrin macrocycle in cobyrinate allows the coordination of thiolates through axial positions (Figure 2A). Heptamethyl cobyrinate perchlorate (Cob(II)) is a tetra-coordinate complex with an open coordination site in the axial position. In the presence of sodium ethanethiolate (NaSEt), the UV−vis absorption spectra of Cob(II) revealed the appearance of new peaks at ∼550 and 600 nm, corresponding to the formation of an axially coordinated Cob(II) complex (Figure S4A). Similarly, we observed the coordination of the thiolate to heptamethyl cyanocobyrinate (Cob(III)−CN), forming a biaxially coordinated complex. The absorption spectra of Cob(III)−CN in the presence of thiolates showed a red-shift in the soret band from 350 to 380 nm and in the $\alpha\beta$ region from 530 to 600 nm compared to the absorption of Cob(III)−CN (Figure 2B, left panel; Figure S4B).

Subsequent irradiation of Cob(III)−thiolate under red light formed a monoaxially coordinated Cob(II) complex via excited-state LMCT to cleave the Co−S bond. The appearance of a new absorption profile with a peak maximum at ∼470 nm indicates photoreduction to Cob(II) (Figure 2B, right panel). In addition, the peaks at ∼550 and 590 nm suggest coordination through the axial position. No further change in the spectral features of the complex was detected upon irradiation for a prolonged time under red light. This observation suggests that the excited state LMCT reactivity of cobyrinate enables a selective reduction of the complex to Cob(II) without undergoing reduction to Cob(I).

We confirmed the photoreduction of the Cob(III)−thiolate complex using electron paramagnetic resonance (EPR) spectroscopy, which revealed the formation of a paramagnetic Cob(II) species upon light irradiation (Figure 2C). The X-band EPR spectra of the photochemically reduced complex showed line splitting due to the hyperfine coupling to ^{59}Co (I = 7/2) with a coupling constant of A_z(Co) = 248.4 MHz. The EPR spectra of the complex suggest coordination of the thiolate ligand through the axial position, showing a lower hyperfine splitting constant compared to that of uncoordinated Cob(II) (Figures S25 and S26).

Electrochemical Studies. Cyclic voltammetry (CV) studies show the effect of tuning the axial coordination of cobyrinate in altering its electronic properties.[38] Examining the electrochemical behavior of Cob(II) possessing no axial ligands revealed a reduction potential of E_p = −310 mV (vs. Fc/Fc$^+$) for the Cob(III)/Cob(II) redox event in *N*,*N*-dimethylformamide (DMF) (Figure 3A, peak a). Further reduction of the Cob(II) complex (without an axial ligand) to Cob(I) was observed at $E_{1/2}$ = −1.07 V (vs Fc/Fc$^+$, Figure 3A, peak b).

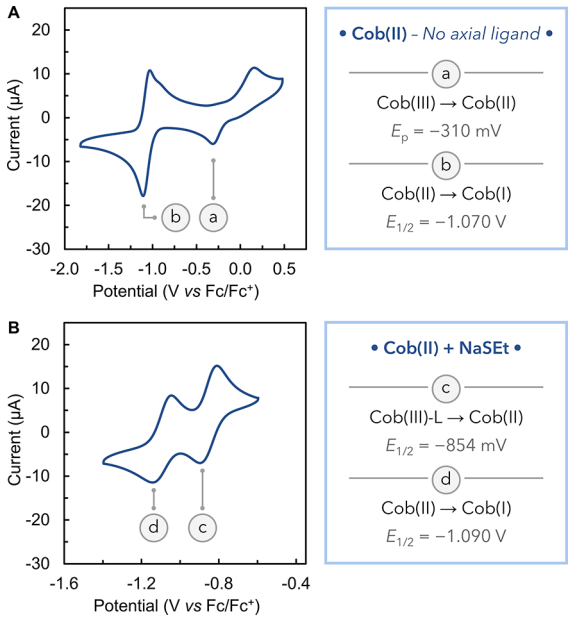

Figure 3. Cyclic voltammograms of Cob(II): (A) in the absence of an additional ligand and (B) in the presence of sodium ethanethiolate (NaSEt) as the axial ligand. The CV measurements were performed in a solution of DMF containing $TBAPF_6$ as the electrolyte at a scan rate of 0.1 V/s ([Cob] = 2 mM, [NaSEt] = 20 mM, and [$TBAPF_6$] = 0.2 mM).

The addition of donor ligands increased the reduction potential of the complex to more negative values. We identified that in the presence of NaSEt, the complex showed a reduction potential of $E_{1/2}$ = −854 mV (vs Fc/Fc$^+$) corresponding to a monoaxially coordinated Cob(III)/Cob(II) redox cycle in DMF (Figure 3B, peak c). The CV spectra of this complex further showed the reduction of the axially uncoordinated Cob(II) to Cob(I) at $E_{1/2}$ = −1.09 V (vs Fc/Fc$^+$, Figure 3B, peak d). Coordination of the thiolate ligand in both axial positions further shifted the reduction potential of Cob(III) to even more negative values at −1.65 V (vs Fc/Fc$^+$), while the reduction of a monoaxially coordinated Cob(II) species to Cob(I) was observed at −1.95 V (vs Fc/Fc$^+$) (Figure S30). This increase in the reduction potential of the complex in the presence of a thiolate axial ligand indicates its enhanced reactivity in polymerization catalysis.

DFT Calculations. We evaluated the excited state reactivity of cobyrinate and the relevance of axial ligands in the homolytic cleavage of the Co−ligand bond via DFT calculations (Figure 4). Using a simplified cobyrinate model, the complex was optimized on Gaussian 16 with the hybrid functional PBE1PBE and the 6-311G(d,p) basis set.[39] The bond dissociation energy (BDE) for the homolysis of the Co−

https://doi.org/10.1021/jacs.4c12432
J. Am. Chem. Soc. 2024, 146, 34583−34590

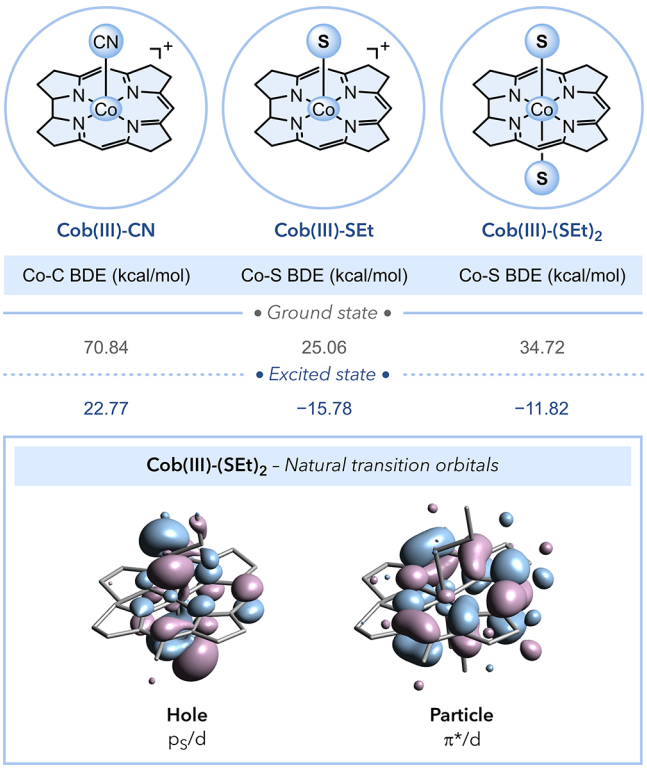

Figure 4. Bond dissociation energy (BDE) of the axially coordinated cobyrinate complexes was calculated via DFT in both the ground and excited states using the PBE1PBE/6-311G(d,p) level. The natural transition orbital (NTO) diagram of the Cob(III)−$(SEt)_2$ complex calculated using the PBE1PBE/6-311+G** level of theory shows a ligand-to-metal charge transfer involving the orbitals of the sulfur atom to cobalt and the macrocycle.

ligand bond was calculated to be 70.84 kcal/mol in the presence of a cyanide ligand (Cob(III)−CN) whereas the coordination of a thiolate ligand (Cob(III)−SEt) decreased the BDE to 25.06 kcal/mol. The natural transition orbitals (NTOs) of the monoaxially coordinated thiolate complex mainly showed a metal-to-ligand charge transfer character, with a minor contribution from LMCT (see SI and Figures S66 and S68 for further details). The calculated excited state BDE of the Co−S bond in the Cob(III)−SEt complex (−15.78 kcal/mol) suggests a thermodynamically favorable process. However, the reduction of the monoaxially coordinated complex (Cob(III)−SEt) forms a Cob(II) species without an axial ligand, whose electronic properties are not suitable for performing ATRP catalysis.

In contrast, the biaxially coordinated complex revealed LMCT character as the major transition in the excited state. The NTOs of the excited state Cob(III)−$(SEt)_2$ show a transfer of electron density from the p-orbitals of the sulfur atom to cobalt's d-orbitals and the π^* of the macrocycle.[36,40] The excited state BDE for the homolysis of the Co−S bond is calculated as −11.82 kcal/mol, which forms an axially ligated Cob(II) complex upon reduction. This observation is further corroborated by the cyclic voltammetry and polymerization studies that suggest the importance of axial ligands in affording active catalysts for ATRP.

Transient Absorption Spectroscopy. Transient absorption spectroscopy was conducted to elucidate the underlying excited state dynamics of cobyrinate. Excitation of the Cob(II) complex without an axial ligand under red light (600 nm) showed a short lifetime of 35 ps (Figure S35). Using the Cob(III)−CN with a red shift in the absorption spectrum, a biexponential decay was fit with lifetimes of 42 and 315 ps (Figure S36). Upon addition of the thiolate as the axial ligand, both complexes yielded an infinite lifetime component, indicating productive chemistry (Figures S37 and S38). We attribute this excited state reactivity of Cob(III) in the presence of the thiolate to the homolytic cleavage of the Co−S bond, occurring in a 266 ps time scale. The excited state dynamics of the Cob(II) complex with thiolate may be attributed to the dissociation of the axial ligand dissociation (or elongation of the Co−S bond) in a time scale of 130 ps (Figure S37). A change in the transient absorption spectra of Cob(II)-thiolate was observed in the presence of ethyl 2-bromopropionate (EBP), where a forward electron transfer occurred with a lifetime of 61 ps, followed by a back electron transfer with a lifetime of 533 ps (Figure S39). This observation suggests a lack of efficient excited state electron transfer for activating the EBP initiator by cobyrinate.

Axially Coordinated Cobyrinate in ATRP Catalysis. We examined the catalytic activity of the axially coordinated Cob(II) in promoting photoinduced ATRP. Our design strategy uses axially coordinated cobyrinate that undergoes photothermal conversion catalysis, where the resulting thermal gradients enhance the efficiency of the activation of alkyl halides to generate initiating radicals for polymerization (Figure 1). While the deactivation step involves the transfer of bromide to propagating species to complete the catalytic cycle, off-cycle radical termination reactions irreversibly oxidize the activator catalyst and slow down polymerization. Our design strategy exploits the ability of thiolates to axially coordinate to cobyrinate forming a Co−S bond, which can be homolytically cleaved through an excited-state LMCT process to generate the activator catalyst.

Polymerization of methyl acrylate (MA) using Cob(II) and NaSEt in a 1/10 ratio under red light irradiation resulted in 88% monomer conversion in 1 h, yielding polymers with a controlled molecular weight and low dispersity (Figure 5A, entry 1). The addition of tetrabutylammonium bromide (TBABr) enhanced the efficiency of deactivation, yielding polymers with low dispersity values (Figure S42). A control experiment in the dark showed <10% monomer conversion and molecular weights higher than theoretical values, indicating low initiation efficiency (<15%) (Figure 5A, entry 2). In addition, excluding the catalyst or the thiolate ligand showed no monomer conversion, indicating the importance of the axially coordinated cobyrinate in mediating ATRP catalysis (Figure 5A, entry 3, and Figure S53). We attribute the diminished catalytic reactivity of the complex in the absence of a thiolate axial ligand to its low reduction potential, as evidenced by the CV measurements (Figure 3).

The presence of the thiolate axial ligand is critical for catalyst regeneration throughout the polymerization, as radical terminations irreversibly oxidize the activator catalyst to Cob(III), which impedes the progress of polymerization. We posit that the coordination of the thiolate ligand to Cob(III) and subsequent homolysis of the Co−S bond via excited state LMCT regenerate the activator catalyst to drive polymerization to completion. Therefore, low catalyst concentrations (1−5 mol % relative to the initiator) could be used to maintain high monomer conversions and fast polymerization rates. The importance of catalyst regeneration was further demonstrated using Cob(II)-CN, which afforded low monomer conversions

https://doi.org/10.1021/jacs.4c12432
J. Am. Chem. Soc. 2024, 146, 34583−34590

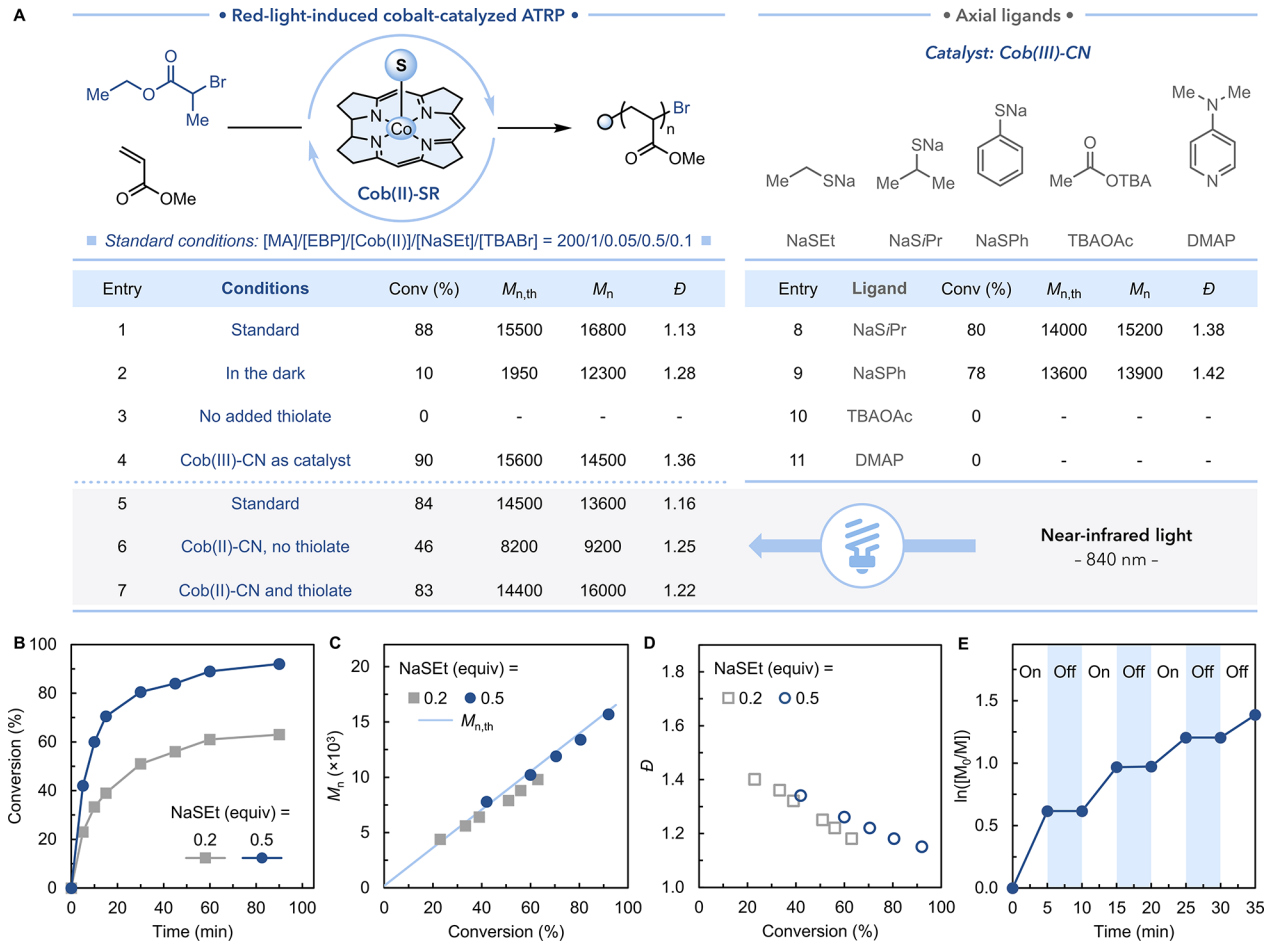

Entry	Conditions	Conv (%)	$M_{n,th}$	M_n	$Đ$
1	Standard	88	15500	16800	1.13
2	In the dark	10	1950	12300	1.28
3	No added thiolate	0	-	-	-
4	Cob(III)-CN as catalyst	90	15600	14500	1.36
5	Standard	84	14500	13600	1.16
6	Cob(II)-CN, no thiolate	46	8200	9200	1.25
7	Cob(II)-CN and thiolate	83	14400	16000	1.22

Entry	Ligand	Conv (%)	$M_{n,th}$	M_n	$Đ$
8	NaS*i*Pr	80	14000	15200	1.38
9	NaSPh	78	13600	13900	1.42
10	TBAOAc	0	-	-	-
11	DMAP	0	-	-	-

Figure 5. (A) Development of cobalt-catalyzed ATRP using axially coordinated cobyrinate under red (630 nm, intensity 0.08 W) or NIR (840 nm, intensity 1.0 W) light irradiation; reaction time 1 h. Effect of the ratio of the thiolate ligand on polymerization of MA: (B) kinetics of the polymerization, (C) evolution of molecular weight (M_n), and (D) dispersity ($Đ$) as a function of monomer conversion. (E) Evidence of temporal control of polymerization kinetics. The equivalency of the thiolate (0.2 and 0.5 equiv) is relative to the EBP initiator with the catalyst used in 0.05 equiv (or 5 mol %).

without the thiolate (Figure S46). The presence of the cyanide ligand makes the catalyst's electronic properties suitable for performing ATRP catalysis under red light.[13] However, due to the lack of catalyst regeneration, only limited monomer conversion was obtained. In contrast, polymerizations reached completion in the presence of thiolates.

In addition, using a Cob(III)−CN complex (heptamethyl cyanocobyrinate) with the thiolate ligand also mediated the polymerization of MA by in situ reduction of the Cob(III)−thiolate complex to activate the alkyl halide initiator (Figure 5A, entry 4). Polymerization of MA using Cob(III)−CN(ClO_4) as the catalyst in the presence of NaSEt resulted in high monomer conversions in polar solvents including DMF, *N*,*N*-dimethylacetamide (DMAc), dimethyl sulfoxide (DMSO), and acetonitrile (ACN) (Figure S50, entries 1−4). Whereas DMF and DMAc yielded polymers with dispersity values ∼1.30, using DMSO as the solvent yielded poor control over molecular weight and dispersity of polymers as the polymerization proceeded fast reaching >80% monomer conversion in 10 min. Moreover, due to the high tendency of DMSO to coordinate to the catalyst, the deactivation of propagating chains via bromine transfer can be inefficient leading to high dispersity values. In contrast, ACN resulted in good control over polymerization with dispersity <1.2. Solvents of low polarity including toluene, tetrahydrofuran (THF), and ethyl acetate (EtOAc) afforded relatively low rates of polymerization and monomer conversions but with good control over molecular weight and low dispersity values (Figure S50 and S51). In contrast to light-induced polymerizations, reactions performed under thermal conditions at 60 °C and excluding light resulted in low monomer conversions and poor control over polymerization (Figure S52). These observations signify the excited state LMCT reactivity of the cobyrinate cleaving the Co−S bond for catalyst regeneration, which cannot be accessed under thermal conditions (Figures S6−S8).

The axially coordinated cobyrinate with thiolate ligands reveals unique reactivity in ATRP catalysis to directly control the catalyst's polymerization behavior with low-energy, red-light irradiation. Previously reported ATRP systems via LMCT regeneration mechanisms typically perform under UV or blue light.[41−43] A photoredox catalytic system is often required to convey the energy of light to transition metal complexes, facilitating polymerization under low-energy light irradiation.[44−48] However, these systems perform polymerization catalysis in the ground state, rendering photochemical control inaccessible. In contrast, modifying the axial coordination of cobyrinate by thiolate ligands unlocked its catalytic potential in ATRP under low-energy light irradiation, while concurrently enabling a photoinduced LMCT process for catalyst

https://doi.org/10.1021/jacs.4c12432
J. Am. Chem. Soc. 2024, 146, 34583−34590

regeneration. We were pleased to demonstrate that this catalytic system also performed well under near-infrared (NIR) light irradiation without requiring additional photosensitizers to activate polymerization (Figure 5A, entries 5−7). The axially coordinated Cob(II) complex shows absorption features in the NIR region at 750−950 nm, enabling the activation of polymerization through photothermal conversion. In the presence of a thiolate ligand, high monomer conversions were achieved under NIR light with reasonable control over the molecular weight and low dispersity of the resulting polymers.

A survey of axial ligands showed that alkyl and aryl thiolates offered well-controlled polymerization of MA under red-light irradiation, yielding ∼80% monomer conversion in 1 h (Figure 5A, entries 1, 8, and 9). We observed the LMCT reactivity of the complex in the presence of a sodium thiophenolate (NaSPh) ligand, albeit with a slower rate of photoreduction compared to alkyl thiolates. Following the photoreduction of a Cob(III) complex in the presence of NaSPh via UV−vis spectroscopy confirmed the low rate of the photoreduction process occurring in ∼30 min under light irradiation (Figures S13−S16). In contrast to thiophenolate, photoreduction of Cob(III) proceeded in <5 min in the presence of alkyl thiolates. DFT calculations show the excited state LMCT and the feasibility of the Co−S bond cleavage in the presence of thiophenolate (Figure S64 and S65). However, due to the low absorption intensity of the LMCT band at ∼600 nm with thiophenolate, the cleavage of the Co−S bond proceeds at a slower rate than that of the alkyl thiolates.

Polymerization of MA using an acetate ligand (i.e., tetrabutylammonium acetate, TBAOAc) showed no reactivity in the presence of Cob(III)−CN (Figure 5A, entry 10). Using the acetate ligand with Cob(II) resulted in 32% monomer conversion with a molecular weight higher than the theoretical value, indicating a low initiator efficiency (Figure S45). Despite the appearance of the spectral features of the complex in the presence of the acetate ligand suggesting coordination to cobyrinate, we did not observe the photoreduction and formation of a Cob(II) complex via the proposed LMCT mechanism to cleave a stronger Co−O bond (Figures S17−S21). This observation was further supported by the control experiments using Cob(III) in conjunction with the acetate, carboxylate, or pyruvate ligands, in which no monomer conversion was obtained under blue-, green-, or red-light irradiation, indicating no photoreduction of the complex (Figure S57).

Using 4-(dimethylamino)pyridine (DMAP) as a neutral donor ligand to both Cob(III)−CN and Cob(II) resulted in no polymerization reactivity or monomer conversion (Figure 5A, entry 11). The CV of the Cob(II) complex in the presence of DMAP showed only a slight change in the reduction potential of the complex, which was lower than that observed with the thiolate ligands (Figure S28). Moreover, the UV−vis spectral features of Cob(III) in the presence of DMAP remained unchanged under light irradiation, indicating a lack of photoreduction (Figures S22−S24). These observations further confirm the unique reactivity of thiolates to modulate the electronic properties of cobyrinate while also enabling LMCT reactivity for catalyst-controlled activator regeneration.

Monitoring the kinetics of the polymerization showed that the polymerization and monomer conversion rate can be increased using higher ratios of the thiolate ligand, which enable continuous catalyst regeneration (Figure 5B-D). Decreasing the catalyst concentration from 5 to 2 and 1 mol % afforded the same polymerization rate and control over molecular weight, albeit with increased dispersity (Figures S41, S60, and S61).

The polymerization kinetics could be temporally controlled on demand via intermittent light on/off periods where the reaction proceeded only under red light irradiation (Figure 5E and Figure S62 and S63). As a photothermal conversion catalyst, cobyrinate generates localized thermal heat gradients, enabling a thermodynamically demanding reaction without raising the bulk temperature (Figure S40). Upon removal of the light source, the thermal gradients rapidly dissipate, allowing control of the kinetics of a thermally driven reaction by light.

CONCLUSIONS

We have developed a strategy to enable the excited state LMCT reactivity of cobyrinate for a catalyst regeneration mechanism in catalyzing ATRP in the presence of thiolates as axial ligands. This catalyst-controlled regeneration mechanism can be accessed across various wavelengths, allowing for efficient and well-controlled polymerization under low-energy light irradiation. Altering the axial coordination of cobyrinate with thiolate ligands was key to modifying the catalyst's structural properties, enabling access to photothermal conversion catalysis and controlling its electronics in mediating ATRP.

ASSOCIATED CONTENT

Supporting Information

The Supporting Information is available free of charge at https://pubs.acs.org/doi/10.1021/jacs.4c12432.

Details of the experimental procedure, supplementary catalyst characterization and polymerization results, and DFT calculations. Additional references cited in the SI.[49−51] (PDF)

AUTHOR INFORMATION

Corresponding Author

Erin E. Stache − *Department of Chemistry, Princeton University, Princeton, New Jersey 08544, United States;* orcid.org/0000-0002-4670-9117; Email: estache@princeton.edu

Authors

Sajjad Dadashi-Silab − *Department of Chemistry, Princeton University, Princeton, New Jersey 08544, United States;* orcid.org/0000-0002-4285-5846

Cristina Preston-Herrera − *Department of Chemistry, Princeton University, Princeton, New Jersey 08544, United States;* orcid.org/0000-0002-0101-2797

Daniel G. Oblinsky − *Department of Chemistry, Princeton University, Princeton, New Jersey 08544, United States;* orcid.org/0000-0001-7460-8260

Gregory D. Scholes − *Department of Chemistry, Princeton University, Princeton, New Jersey 08544, United States;* orcid.org/0000-0003-3336-7960

Complete contact information is available at: https://pubs.acs.org/10.1021/jacs.4c12432

Notes

The authors declare no competing financial interest.

■ ACKNOWLEDGMENTS

Financial support was provided in part by Princeton University and the National Science Foundation under Award CHE-2237784 for polymerization optimization and kinetics studies, and the National Institutes of Health award R35GM150839 for catalyst development and photothermal conversion studies. This work made use of the NMR and Ultrafast Laser Spectroscopy Facilities at Princeton University. We thank the MacMillan Group for using their potentiostat for cyclic voltammetry studies and Dr. Kristen Berger and Dr. Alexandra Brown, for their helpful discussion on the DFT calculations and EPR simulations.

■ REFERENCES

(1) Prier, C. K.; Rankic, D. A.; MacMillan, D. W. C. Visible Light Photoredox Catalysis with Transition Metal Complexes: Applications in Organic Synthesis. *Chem. Rev.* **2013**, *113* (7), 5322−5363.
(2) Romero, N. A.; Nicewicz, D. A. Organic Photoredox Catalysis. *Chem. Rev.* **2016**, *116* (17), 10075−10166.
(3) Chen, M.; Zhong, M.; Johnson, J. A. Light-Controlled Radical Polymerization: Mechanisms, Methods, and Applications. *Chem. Rev.* **2016**, *116* (17), 10167−10211.
(4) Pan, X.; Tasdelen, M. A.; Laun, J.; Junkers, T.; Yagci, Y.; Matyjaszewski, K. Photomediated Controlled Radical Polymerization. *Prog. Polym. Sci.* **2016**, *62*, 73−125.
(5) Schultz, D. M.; Yoon, T. P. Solar Synthesis: Prospects in Visible Light Photocatalysis. *Science* **2014**, *343* (6174), 1239176.
(6) Chan, A. Y.; Ghosh, A.; Yarranton, J. T.; Twilton, J.; Jin, J.; Arias-Rotondo, D. M.; Sakai, H. A.; McCusker, J. K.; MacMillan, D. W. C. Exploiting the Marcus Inverted Region for First-Row Transition Metal-Based Photoredox Catalysis. *Science* **2023**, *382* (6667), 191−197.
(7) McCusker, J. K. Electronic Structure in the Transition Metal Block and Its Implications for Light Harvesting. *Science* **2019**, *363* (6426), 484−488.
(8) Matter, M. E.; Čamdžić, L.; Stache, E. E. Photothermal Conversion by Carbon Black Facilitates Aryl Migration by Photon-Promoted Temperature Gradients. *Angew. Chem., Int. Ed.* **2023**, *62* (40), No. e202308648.
(9) Kugelmass, L. H.; Tagnon, C.; Stache, E. E. Photothermal Mediated Chemical Recycling to Monomers via Carbon Quantum Dots. *J. Am. Chem. Soc.* **2023**, *145* (29), 16090−16097.
(10) Matter, M. E.; Tagnon, C.; Stache, E. E. Recent Applications of Photothermal Conversion in Organic Synthesis. *ACS Cent. Sci.* **2024**, *10* (8), 1460−1472.
(11) Cui, X.; Ruan, Q.; Zhuo, X.; Xia, X.; Hu, J.; Fu, R.; Li, Y.; Wang, J.; Xu, H. Photothermal Nanomaterials: A Powerful Light-to-Heat Converter. *Chem. Rev.* **2023**, *123* (11), 6891−6952.
(12) Song, C.; Wang, Z.; Yin, Z.; Xiao, D.; Ma, D. Principles and Applications of Photothermal Catalysis. *Chem. Catal.* **2022**, *2* (1), 52−83.
(13) Preston-Herrera, C.; Dadashi-Silab, S.; Oblinsky, D. G.; Scholes, G. D.; Stache, E. E. Molecular Photothermal Conversion Catalyst Promotes Photocontrolled Atom Transfer Radical Polymerization. *J. Am. Chem. Soc.* **2024**, *146* (13), 8852−8857.
(14) Dadashi-Silab, S.; Preston-Herrera, C.; Stache, E. E. Vitamin B12 Derivative Enables Cobalt-Catalyzed Atom Transfer Radical Polymerization. *J. Am. Chem. Soc.* **2023**, *145* (35), 19387−19395.
(15) Juliá, F. Ligand-to-Metal Charge Transfer (LMCT) Photochemistry at 3d-Metal Complexes: An Emerging Tool for Sustainable Organic Synthesis. *ChemCatChem.* **2022**, *14* (19), No. e202200916.
(16) Abderrazak, Y.; Bhattacharyya, A.; Reiser, O. Visible-Light-Induced Homolysis of Earth-Abundant Metal-Substrate Complexes: A Complementary Activation Strategy in Photoredox Catalysis. *Angew. Chem., Int. Ed.* **2021**, *60* (39), 21100−21115.
(17) May, A. M.; Dempsey, J. L. A New Era of LMCT: Leveraging Ligand-to-Metal Charge Transfer Excited States for Photochemical Reactions. *Chem. Sci.* **2024**, *15* (18), 6661−6678.
(18) Treacy, S. M.; Rovis, T. Photoinduced Ligand-to-Metal Charge Transfer in Base-Metal Catalysis. *Synthesis* **2024**, *56*, 1967−1978.
(19) Gygi, D.; Gonzalez, M. I.; Hwang, S. J.; Xia, K. T.; Qin, Y.; Johnson, E. J.; Gygi, F.; Chen, Y.-S.; Nocera, D. G. Capturing the Complete Reaction Profile of a C-H Bond Activation. *J. Am. Chem. Soc.* **2021**, *143* (16), 6060−6064.
(20) Chinchole, A.; Henriquez, M. A.; Cortes-Arriagada, D.; Cabrera, A. R.; Reiser, O. Iron(III)-Light-Induced Homolysis: A Dual Photocatalytic Approach for the Hydroacylation of Alkenes Using Acyl Radicals via Direct HAT from Aldehydes. *ACS Catal.* **2022**, *12* (21), 13549−13554.
(21) Bian, K.-J.; Kao, S.-C.; Nemoto, D.; Chen, X.-W.; West, J. G. Photochemical Diazidation of Alkenes Enabled by Ligand-to-Metal Charge Transfer and Radical Ligand Transfer. *Nat. Commun.* **2022**, *13* (1), 7881.
(22) Lu, Y.-C.; West, J. G. Chemoselective Decarboxylative Protonation Enabled by Cooperative Earth-Abundant Element Catalysis. *Angew. Chem., Int. Ed.* **2023**, *62* (3), No. e202213055.
(23) Oh, S.; Stache, E. E. Chemical Upcycling of Commercial Polystyrene via Catalyst-Controlled Photooxidation. *J. Am. Chem. Soc.* **2022**, *144* (13), 5745−5749.
(24) Treacy, S. M.; Rovis, T. Copper Catalyzed C(Sp3)-H Bond Alkylation via Photoinduced Ligand-to-Metal Charge Transfer. *J. Am. Chem. Soc.* **2021**, *143* (7), 2729−2735.
(25) Xu, P.; López-Rojas, P.; Ritter, T. Radical Decarboxylative Carbometalation of Benzoic Acids: A Solution to Aromatic Decarboxylative Fluorination. *J. Am. Chem. Soc.* **2021**, *143* (14), 5349−5354.
(26) Li, Q. Y.; Gockel, S. N.; Lutovsky, G. A.; DeGlopper, K. S.; Baldwin, N. J.; Bundesmann, M. W.; Tucker, J. W.; Bagley, S. W.; Yoon, T. P. Decarboxylative Cross-Nucleophile Coupling via Ligand-to-Metal Charge Transfer Photoexcitation of Cu(Ii) Carboxylates. *Nat. Chem.* **2022**, *14* (1), 94−99.
(27) Dow, N. W.; Pedersen, P. S.; Chen, T. Q.; Blakemore, D. C.; Dechert-Schmitt, A.-M.; Knauber, T.; MacMillan, D. W. C. Decarboxylative Borylation and Cross-Coupling of (Hetero)Aryl Acids Enabled by Copper Charge Transfer Catalysis. *J. Am. Chem. Soc.* **2022**, *144* (14), 6163−6172.
(28) Shields, B. J.; Doyle, A. G. Direct C(Sp3)-H Cross Coupling Enabled by Catalytic Generation of Chlorine Radicals. *J. Am. Chem. Soc.* **2016**, *138* (39), 12719−12722.
(29) Hwang, S. J.; Powers, D. C.; Maher, A. G.; Anderson, B. L.; Hadt, R. G.; Zheng, S.-L.; Chen, Y.-S.; Nocera, D. G. Trap-Free Halogen Photoelimination from Mononuclear Ni(III) Complexes. *J. Am. Chem. Soc.* **2015**, *137* (20), 6472−6475.
(30) Ackerman, L. K. G.; Martinez Alvarado, J. I.; Doyle, A. G. Direct C-C Bond Formation from Alkanes Using Ni-Photoredox Catalysis. *J. Am. Chem. Soc.* **2018**, *140* (43), 14059−14063.
(31) Kariofillis, S. K.; Doyle, A. G. Synthetic and Mechanistic Implications of Chlorine Photoelimination in Nickel/Photoredox C(Sp3)-H Cross-Coupling. *Acc. Chem. Res.* **2021**, *54* (4), 988−1000.
(32) Hu, A.; Guo, J.-J.; Pan, H.; Tang, H.; Gao, Z.; Zuo, Z. δ-Selective Functionalization of Alkanols Enabled by Visible-Light-Induced Ligand-to-Metal Charge Transfer. *J. Am. Chem. Soc.* **2018**, *140* (5), 1612−1616.
(33) Zhang, K.; Chang, L.; An, Q.; Wang, X.; Zuo, Z. Dehydroxymethylation of Alcohols Enabled by Cerium Photocatalysis. *J. Am. Chem. Soc.* **2019**, *141* (26), 10556−10564.
(34) Conrad, K. S.; Brunold, T. C. Spectroscopic and Computational Studies of Glutathionylcobalamin: Nature of Co-S Bonding and Comparison to Co-C Bonding in Coenzyme B12. *Inorg. Chem.* **2011**, *50* (18), 8755−8766.
(35) Tahara, K.; Matsuzaki, A.; Masuko, T.; Kikuchi, J.; Hisaeda, Y. Synthesis, Characterization, Co-S Bond Reactivity of a Vitamin B12 Model Complex Having Pentafluorophenylthiolate as an Axial Ligand. *Dalton Trans.* **2013**, *42* (18), 6410−6416.

(36) Toda, M. J.; Lodowski, P.; Thurman, T. M.; Kozlowski, P. M. Light Mediated Properties of a Thiolato-Derivative of Vitamin B12. *Inorg. Chem.* **2020**, *59* (23), 17200−17212.
(37) Li, Z.; Mascarenhas, R.; Twahir, U. T.; Kallon, A.; Deb, A.; Yaw, M.; Penner-Hahn, J.; Koutmos, M.; Warncke, K.; Banerjee, R. An Interprotein Co-S Coordination Complex in the B12-Trafficking Pathway. *J. Am. Chem. Soc.* **2020**, *142* (38), 16334−16345.
(38) Giedyk, M.; Shimakoshi, H.; Goliszewska, K.; Gryko, D.; Hisaeda, Y. Electrochemistry and Catalytic Properties of Amphiphilic Vitamin B12 Derivatives in Nonaqueous Media. *Dalton Trans.* **2016**, *45* (20), 8340−8346.
(39) Chemaly, S. M.; Brown, K. L.; Fernandes, M. A.; Munro, O. Q.; Grimmer, C.; Marques, H. M. Probing the Nature of the CoIII Ion in Corrins: The Structural and Electronic Properties of Dicyano- and Aquacyanocobyrinic Acid Heptamethyl Ester and a Stable Yellow Dicyano- and Aquacyanocobyrinic Acid Heptamethyl Ester. *Inorg. Chem.* **2011**, *50* (18), 8700−8718.
(40) Eisenberg, A. S.; Likhtina, I. V.; Znamenskiy, V. S.; Birke, R. L. Electronic Spectroscopy and Computational Studies of Glutathionylco(III)Balamin. *J. Phys. Chem. A* **2012**, *116* (25), 6851−6869.
(41) Pan, X.; Malhotra, N.; Zhang, J.; Matyjaszewski, K. Photoinduced Fe-Based Atom Transfer Radical Polymerization in the Absence of Additional Ligands, Reducing Agents, and Radical Initiators. *Macromolecules* **2015**, *48* (19), 6948−6954.
(42) Dadashi-Silab, S.; Pan, X.; Matyjaszewski, K. Photoinduced Iron-Catalyzed Atom Transfer Radical Polymerization with Ppm Levels of Iron Catalyst under Blue Light Irradiation. *Macromolecules* **2017**, *50* (20), 7967−7977.
(43) Szczepaniak, G.; Łagodzińska, M.; Dadashi-Silab, S.; Gorczyński, A.; Matyjaszewski, K. Fully Oxygen-Tolerant Atom Transfer Radical Polymerization Triggered by Sodium Pyruvate. *Chem. Sci.* **2020**, *11* (33), 8809−8816.
(44) Pan, X.; Fantin, M.; Yuan, F.; Matyjaszewski, K. Externally Controlled Atom Transfer Radical Polymerization. *Chem. Soc. Rev.* **2018**, *47* (14), 5457−5490.
(45) Lorandi, F.; Fantin, M.; Matyjaszewski, K. Atom Transfer Radical Polymerization: A Mechanistic Perspective. *J. Am. Chem. Soc.* **2022**, *144* (34), 15413−15430.
(46) Kütahya, C.; Schmitz, C.; Strehmel, V.; Yagci, Y.; Strehmel, B. Near-Infrared Sensitized Photoinduced Atom-Transfer Radical Polymerization (ATRP) with a Copper(II) Catalyst Concentration in the Ppm Range. *Angew. Chem., Int. Ed.* **2018**, *57* (26), 7898−7902.
(47) Dadashi-Silab, S.; Lorandi, F.; DiTucci, M. J.; Sun, M.; Szczepaniak, G.; Liu, T.; Matyjaszewski, K. Conjugated Cross-Linked Phenothiazines as Green or Red Light Heterogeneous Photocatalysts for Copper-Catalyzed Atom Transfer Radical Polymerization. *J. Am. Chem. Soc.* **2021**, *143* (25), 9630−9638.
(48) Hu, X.; Szczepaniak, G.; Lewandowska-Andralojc, A.; Jeong, J.; Li, B.; Murata, H.; Yin, R.; Jazani, A. M.; Das, S. R.; Matyjaszewski, K. Red-Light-Driven Atom Transfer Radical Polymerization for High-Throughput Polymer Synthesis in Open Air. *J. Am. Chem. Soc.* **2023**, *145* (44), 24315−24327.
(49) Snellenburg, J. J.; Laptenok, S.; Seger, R.; Mullen, K. M.; van Stokkum, I. H. M. Glotaran: A Java-Based Graphical User Interface for the R Package TIMP. *J. Stat. Softw.* **2012**, *49*, 1−22.
(50) Ociepa, M.; Wierzba, A. J.; Turkowska, J.; Gryko, D. Polarity-Reversal Strategy for the Functionalization of Electrophilic Strained Molecules via Light-Driven Cobalt Catalysis. *J. Am. Chem. Soc.* **2020**, *142* (11), 5355−5361.
(51) Murakami, Y.; Hisaeda, Y.; Kajihara, A. Hydrophobic Vitamin B12. I. Preparation and Axial Ligation Behavior of Hydrophobic Vitamin B12r. *Bull. Chem. Soc. Jpn.* **1983**, *56* (12), 3642−3646.

https://doi.org/10.1021/jacs.4c12432
J. Am. Chem. Soc. 2024, 146, 34583−34590